Applied Catalysis B: Environmental 307 (2022) 121204

Contents lists available at ScienceDirect

Applied Catalysis B: Environmental

journal homepage: www.elsevier.com/locate/apcatb

Ru-incorporated oxygen-vacancy-enriched MoO_2 electrocatalysts for hydrogen evolution reaction

Chuang Li [a,1], Haeseong Jang [b,1], Min Gyu Kim [c], Liqiang Hou [a,*], Xien Liu [a,*], Jaephil Cho [b,*]

[a] State Key Laboratory Based of Eco-Chemical Engineering, College of Chemical Engineering, Qingdao University of Science and Technology, Qingdao 266042, PR China
[b] Department of Energy Engineering, Department of Energy and Chemical Engineering, Ulsan National Institute of Science and Technology (UNIST) Ulsan, 44919, South Korea
[c] Beamline Research Division, Pohang Accelerator Laboratory (PAL), Pohang 37673, Korea

ARTICLE INFO

Keywords:
Ru nanocluster
Transition
Oxygen vacancies
Ru-O-Mo sites
Hydrogen evolution reaction

ABSTRACT

Designing highly efficient Pt-free electrocatalysts with low overpotential for the alkaline hydrogen evolution reaction (HER) remains a significant challenge. In this paper, we successfully construct Ru-incorporated oxygen-vacancy-enriched MoO_2 nanosheets (Ru/MoO_{2-x}) for the HER through a "one stone two birds" strategy. This strategy can solve two urgent problems simultaneously, the intrinsic electrochemical activity of original MoO_2 is far from satisfactory and the H_2O adsorption/dissociation abilities of Ru are weak. Specifically, the oxygen-vacancy-enriched MoO_3 serves as an excellent platform for anchoring and trapping Ru ions. In-depth analyses indicate that the incorporation of Ru nanoclusters induces transition from MoO_3 to MoO_2, generates oxygen vacancies, and creates Ru-O-Mo sites. The synergistic effect of Ru nanoclusters, Ru-O-Mo sites and oxygen-vacancy-enriched MoO_2 will endow the obtained catalyst excellent electrocatalytic activity. In particular, the optimal Ru/MoO_{2-x} electrocatalyst delivered a low overpotential of 29 mV at 10 mA cm^{-2} in a basic electrolyte.

1. Introduction

Owing to its reproducible and eco-friendly properties compared to those of other fuels, hydrogen is considered as a sustainable alternative to meet future global energy demands [1–3]. Compared to traditional technologies, electrochemical water splitting is a promising and efficient strategy for producing green hydrogen [4–9]. At present, noble metal Pt or Pt-based catalysts are the most efficient electrocatalysts used for the hydrogen evolution reaction (HER). Nevertheless, their high price and rareness impede their wholesale practical utilization [1,10–12]. The exploration of efficient Pt-free electrocatalysts for the HER is significantly challenging. The overpotential of the HER in acidic media is generally lower than that in alkaline media. However, the HER in alkaline media is promising, because the best catalysts that produce oxygen in another half-reaction of water splitting always catalyze efficiently in alkaline or neutral solutions [13–16]. Therefore, exploring inexpensive and efficient Pt-free electrocatalysts for the HER in alkaline media is desirable.

Recently, low-cost Mo-based catalysts (MoO_2 [17,18], MoO_3 [13], and MoS_2 [19], etc.) and Ru-based catalysts [4] have been extensively explored as alternatives to Pt. Thereinto, MoO_2 with a tortile rutile type structure is a potential alternative to Pt-based catalysts for the HER, owing to its excellent electrochemical activity, and high chemical stability [20,21]. However, the intrinsic electrochemical activity of pure MoO_2 is far from satisfactory. Generally, the catalytic activity of MoO_2 can be favorably enhanced via metal hybridization and defect engineering [22–24]. Oxygen vacancy engineering on MoO_2 can regulate its electronic structure, enhancing its catalytic activities [23–26]. Similarly, metal hybridization is believed to modulate the electron density of materials to regulate their catalytic properties [17,27–29]. Ru is another potential alternative to Pt for the HER, because of its lower price (1/2 times the cost of the Pt metal) and similar hydrogen intermediate (H*) adsorption energy compared to Pt [30,31]. Nevertheless, the faint H_2O adsorption and dissociation abilities of Ru significantly deteriorate its intrinsic activity in the alkaline HER [32,33]. Oxygen doping and/or the build of adequately Ru-O-M (M means Metal) sites can regulate the charge distribution to modulate the coordination environment of Ru at the interface and is an effective means for enhancing the activity of Ru [34,35].

Thought-provoking, if we combine Ru with MoO_2, MoO_2 can provide

* Corresponding authors.
E-mail addresses: houliqiang@qust.edu.cn (L. Hou), liuxien@qust.edu.cn (X. Liu), jpcho@unist.ac.kr (J. Cho).
[1] C. Li and H. Jang contributed equally to this work.

https://doi.org/10.1016/j.apcatb.2022.121204
Received 4 November 2021; Received in revised form 8 February 2022; Accepted 9 February 2022
Available online 11 February 2022

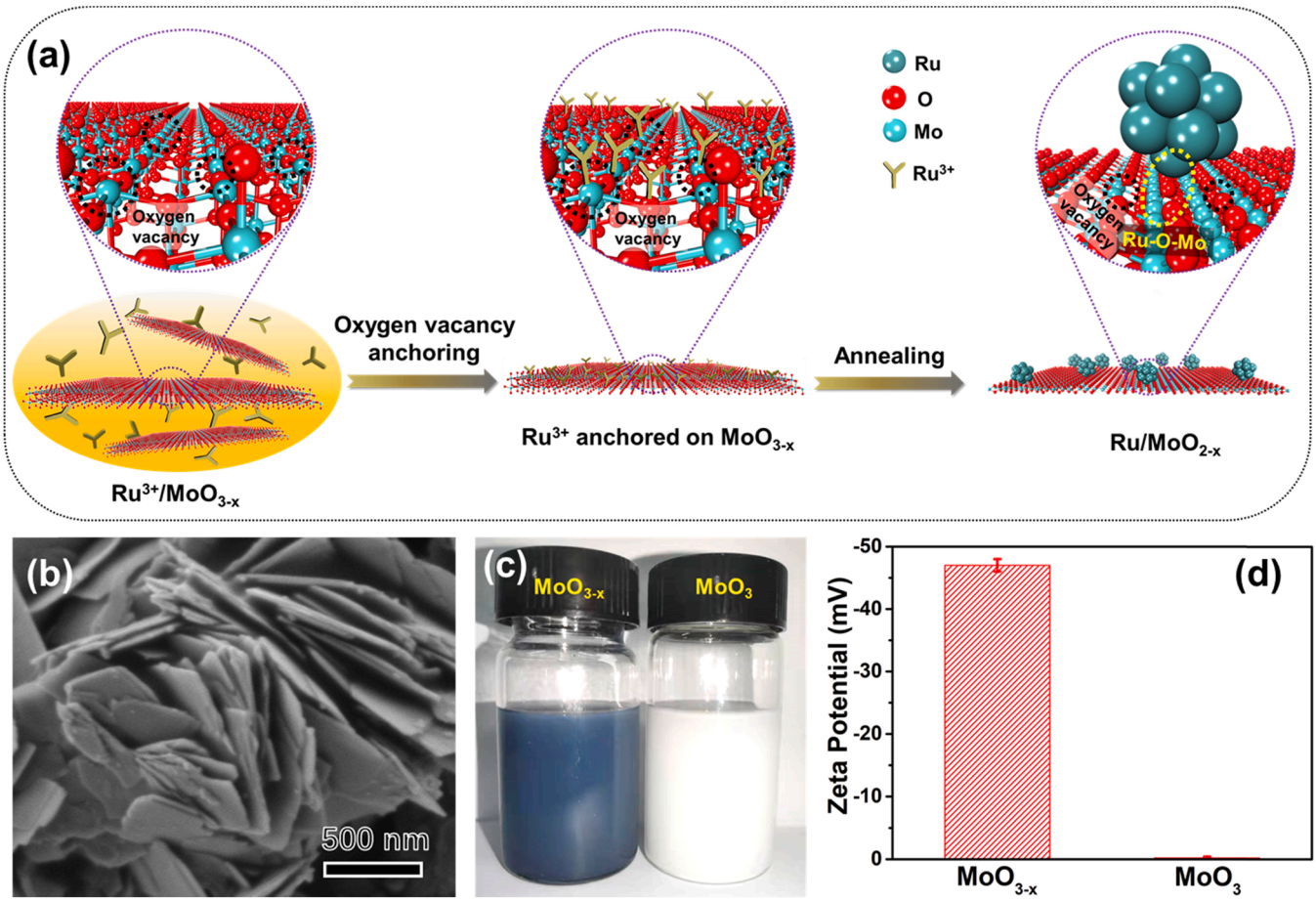

Fig. 1. (a) Schematic illustration of the preparation for Ru/MoO_{2-x}. (b) SEM image of MoO_{3-x}. (c) The photographs of the MoO_{3-x} and MoO_3 powder dispersed in ethanol. (d) Comparison of zeta potential of MoO_{3-x} and MoO_3.

whether oxygen to bond Ru atom to generate Ru-O-Mo site, and simultaneously construct oxygen vacancy in MoO_2, realizing one stone two birds? In this study, we successfully designed and incorporated Ru nanoclusters on oxygen-vacancy-enriched MoO_2 nanosheets (Ru/MoO_{2-x}). Previous researches have demonstrated that the oxygen vacancies on metal oxides can be used as anchoring sites for the adsorption of metal cations to realize the loading of other metals [23,25,36,37]. Therefore, to successfully prepare Ru/MoO_{2-x} catalyst, we propose a strategy by adopting oxygen-vacancy-enriched MoO_3 as an anchoring substrate to couple the Ru cation, followed by annealing treatment. Detailed analyses reveal that the incorporated Ru nanoclusters can promote the transformation from MoO_3 to MoO_2, and the generation of oxygen vacancies, benefiting the HER. Meanwhile, the incorporation of Ru induces the formation of the Ru-O-Mo sites to further enhance the catalytic activity of the Ru/MoO_{2-x} for the HER. In particular, the optimal catalyst exhibits an overpotential of 29 mV at a current density of 10 mA cm^{-2}, with a Tafel slope of 22 mV dec^{-1} in 1 M KOH electrolyte.

2. Experimental sections

2.1. Materials and chemicals

$RuCl_3{\cdot}xH_2O$ was purchased from Aladdin. Molybdenum powder was purchased from Macklin. Hydrogen peroxide 30% aqueous solution and ethanol were obtained from Sinopharm Chemical Reagent Co.,Ltd. All chemicals were used without further purification.

2.2. Synthesis of Ru/MoO_{2-x} catalysts

First, the substrate of oxygen-vacancy-enriched molybdenum trioxide nanosheet (MoO_{3-x}) was prepared using hydrothermal process as previously reported method [38]. The Ru/MoO_{2-x} catalyst was prepared using the following method. First, 30 mg of MoO_{3-x} nanosheet was dispersed in 5 mL of deionized water and stirred for 30 min. Thereafter, 1 mL of a $RuCl_3{\cdot}xH_2O$ (5 mg mL^{-1}) solution was added to the MoO_{3-x} solution and keep stirring at room temperature for 12 h. The precursor was collected by centrifugation, rinsed three times with deionized water, and dried at 60 °C under vacuum for 12 h. Finally, the precursor was annealed in a tube furnace at 350 °C for 2 h at a heating rate of 5 °C min^{-1} under an Ar/H_2 (95/5) atmosphere to obtain Ru/MoO_{2-x}. For comparison, MoO_{3-x} nanosheet was annealed under the same conditions with Ru/MoO_{2-x}, and the final product was defined as A-MoO_{3-x}. The precursor was also annealed at 200, 550 and 700 °C to prepare Ru/MoO_{2-x}-200, Ru/MoO_{2-x}-550 and Ru/MoO_{2-x}-700, respectively. In addition, the Ru/MoO_{2-x}-2 mg and Ru/MoO_{2-x}-10 mg were synthesized by adding 2 and 10 mg mL^{-1} of $RuCl_3{\cdot}xH_2O$ solutions, respectively.

2.3. Composition and structural characterizations

X-ray diffraction (XRD) and X-ray photoelectron spectroscopy (XPS) spectra were performed on the catalyst using a D/Max2000, diffractometer with Cu Kα radiation, and an Escalab instrument with the model of Escalab 250 xi (Thermo Scientific, England), respectively. The morphologies of the obtained samples were analyzed by field-emission scanning electron microscopy (FE-SEM) using a Hitachi S4800

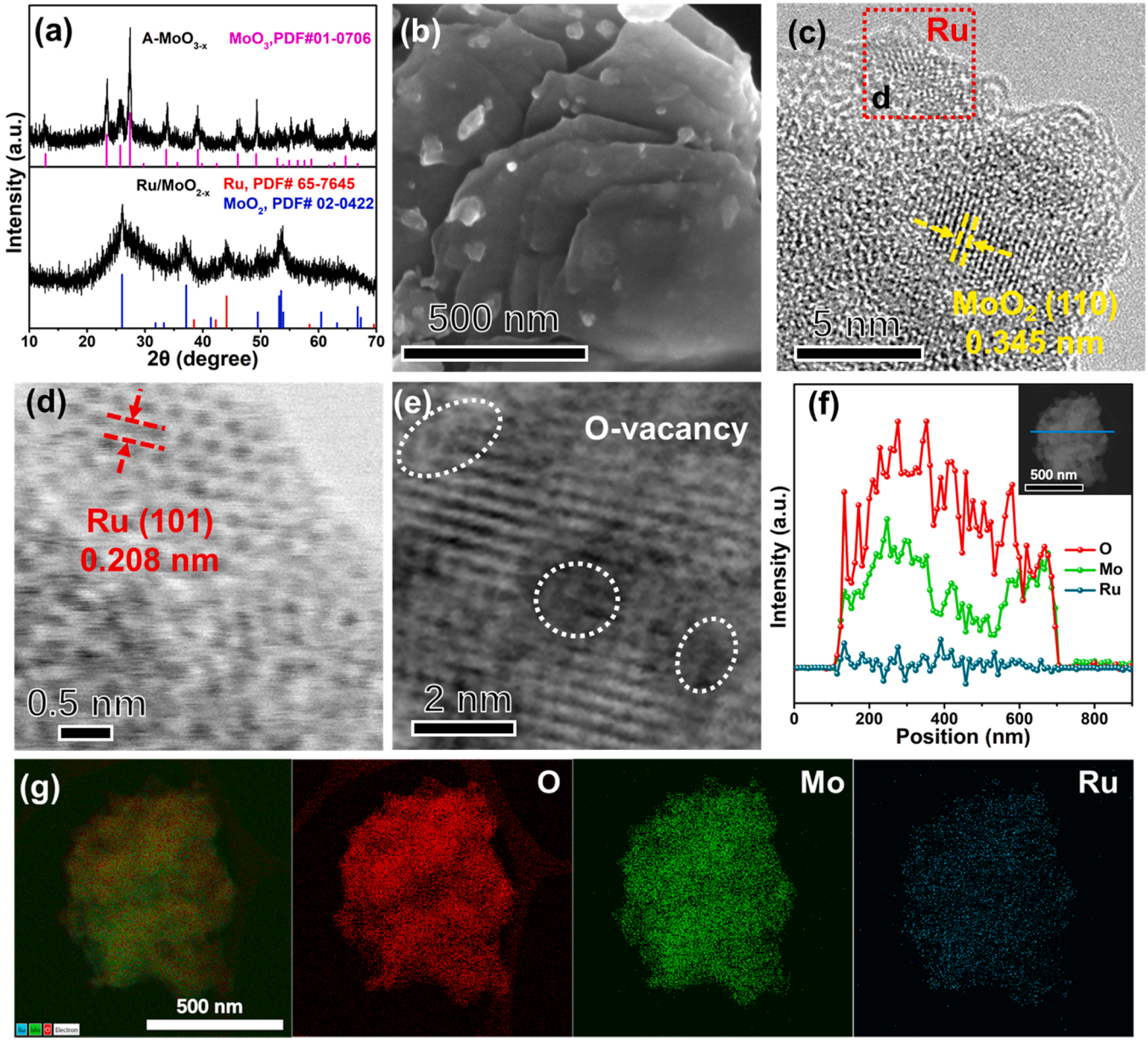

Fig. 2. (a) XRD pattern, (b) SEM, (c) HRTEM, (d, e) ADF-STEM images, (f) EDX line scanning image (inset: ADF-STEM image showing the line scanned) (g) Overlap mapping image and element mapping of Ru/MoO_{2-x}.

microscope, Transmission electron microscopy (TEM), and high-resolution TEM (HRTEM) were performed using a JEOL JEM-2100 F transmission electron microscope. The BL10C beamline at the Pohang Light Source (PLS-II) in Korea was used to measure the X-ray absorption near-edge structure (XANES) and extended X-ray absorption fine structure (EXAFS) spectra.

2.4. Electrochemical experiments

Electrochemical measurements were performed using a conventional three-electrode configuration on a CHI 760E electrochemical workstation (CHI Instruments, China). A graphite rod and a reversible hydrogen electrode were used as the counter electrode and reference electrode, respectively. The catalyst ink was prepared as follows: 2 mg of the sample, 2 mg of XC-72, and 40 μL of 5 wt% Nafion solution were dispersed in 300 μL of anhydrous ethanol through sonication for at least 1 h. Subsequently, 6 μL of the catalyst ink was dropped onto the surface of a glassy carbon electrode with a diameter of 5 mm. For the HER, linear sweep voltammetry at a scan rate of 5 mV s^{-1} was conducted in 1 M KOH for all samples, and data were obtained with IR compensation of 95%.

3. Results and discussion

3.1. Morphology and structure characterizations

Considering the adsorption effect of metal cations on oxygen-vacancy-enriched metal oxides, we choose oxygen-vacancy-enriched MoO_3 (MoO_{3-x}) as the substrate to prepare an excellent catalyst, as shown in Fig. 1. The precursor MoO_{3-x} is synthesized by a solvent thermal method. Then, the Ru^{3+} is anchored on the MoO_{3-x} (Ru^{3+}/MoO_{3-x}) using wet impregnation since oxygen vacancies that served as anchoring sites for metal cation are abundantly present. Finally, the Ru nanoclusters anchored on oxygen-vacancy-enriched MoO_2 (Ru/MoO_{2-x}) is in-situ synthesized by annealing the Ru^{3+}/MoO_{3-x} under an Ar/H_2 atmosphere.

The XRD analysis of MoO_{3-x} substrate reveals the present

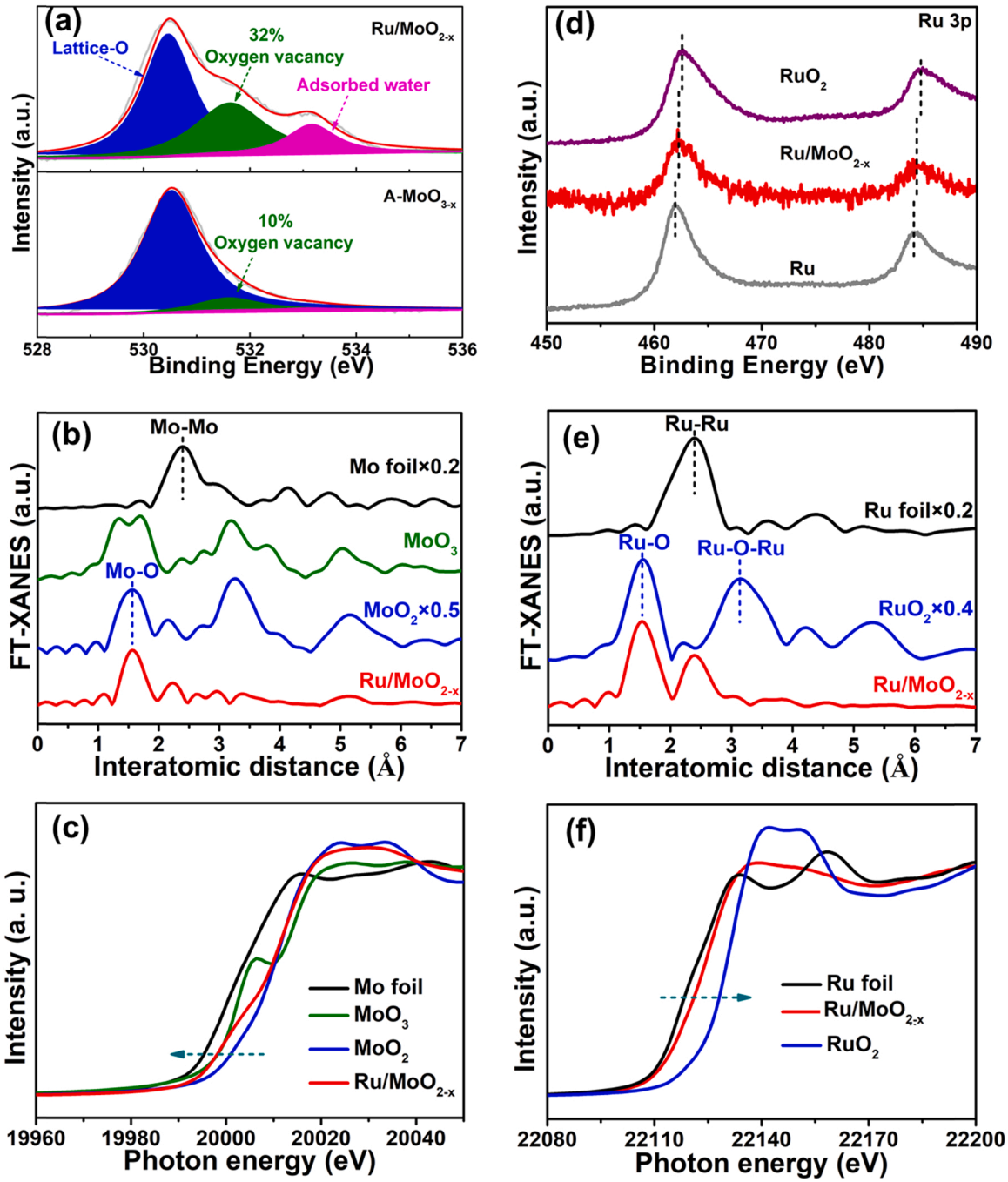

Fig. 3. (a) XPS spectra of O 1 s of A-MoO_{3-x} and Ru/MoO_{2-x}. The Mo K-edge (b) EXAFS and (c) XANES spectra of Ru/MoO_{2-x}, Mo foil, MoO_2, and MoO_3. (d) The comparison of XPS spectra of Ru 3p for metal Ru, Ru/MoO_{2-x} and RuO_2. The Ru K-edge (e) EXAFS and (f) XANES spectra of Ru/MoO_{2-x}, Ru foil, and RuO_2.

orthorhombic phase (PDF#05–0508) corresponding to MoO_3 (Fig. S1). SEM image (Fig. 1b) presents the MoO_{3-x} substrate with two-dimensional nanosheets. In addition, as shown in Fig. S2a, the high-resolution Mo 3d signal from the MoO_{3-x} substrate can be deconvoluted into four typical components corresponding to Mo^{5+} $3d_{3/2}$, Mo^{6+} $3d_{3/2}$, Mo^{5+} $3d_{5/2}$, and Mo^{6+} $3d_{5/2}$. The low-valence states of Mo^{5+} imply the formation of MoO_{3-x} with oxygen vacancies, which is also ensured by the O 1 s XPS spectra (Fig. S2b) [13,38,39]. Additionally, the concentration of oxygen vacancies is as high as 30%. Moreover, as observed in Fig. 1c, the MoO_{3-x} substrate exhibits a blue color, which will turn white after suffering annealing at 460 °C in air (defined as MoO_3), further proving the existence of oxygen vacancies [13,38]. The above results indicate that the oxygen-vacancy-enriched MoO_3 nanosheets are successfully prepared. Zeta potential measurements (Fig. 1d) show that the zeta potential value for MoO_{3-x} is − 47 mV, while the zeta potential value for MoO_3 is almost zero, indicating that the surface of MoO_{3-x} is negatively charged in deionized water. Namely, the abundant oxygen vacancies will endow MoO_{3-x} with a large negative charge, thus providing plentiful anchoring sites to absorb Ru^{3+}. To better demonstrate the effect of oxygen vacancy, we also choose MoO_3 as substrate. After static settlement, there is an obvious difference for the liquid supernatant as shown in Fig. S3a, indicating that the oxygen-vacancy-enriched MoO_3 is more beneficial to anchoring the Ru^{3+}. After annealing treatment, the content of Ru on MoO_3 is lower than that on MoO_{3-x} substrate (Fig. S3b-c), resulting in an inferior performance for HER (Fig. S3d).

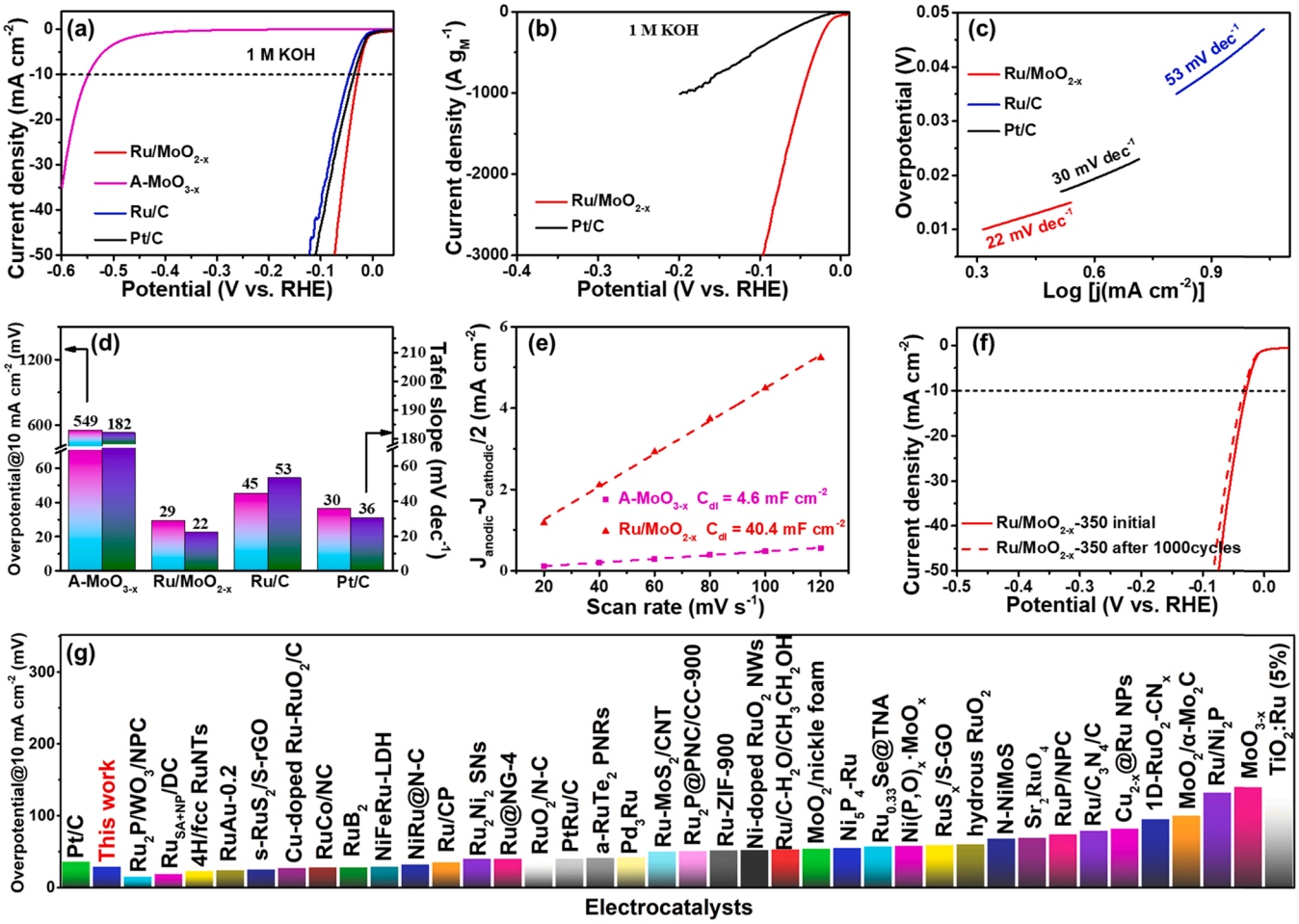

Fig. 4. (a) LSV curves of Ru/MoO_{2-x}, A-MoO_{3-x}, Ru/C, and commercial Pt/C catalyst in 1 M KOH. (b) The mass activities of Ru/MoO_{2-x} and Pt/C. (c) Tafel slopes of Ru/MoO_{2-x}, Ru/C, and commercial Pt/C derived from Polarization curves in Fig. 4a. (d) The histograms of overpotential and Tafel slopes for Ru/MoO_{2-x}, A-MoO_{3-x}, 5 wt% Ru/C, and commercial 20 wt% Pt/C catalyst. (e) C_{dl} of Ru/MoO_{2-x} and A-MoO_{3-x}. (f) Durability of Ru/MoO_{2-x} for 1000 cycles CV cycles in 1 M KOH. (g) Overpotentials at a current density of 10 mA cm^{-2} for Ru/MoO_{2-x} and the reported catalysts.

The optimal Ru/MoO_{2-x} catalyst is prepared by annealing the precursor Ru^{3+}/MoO_{3-x} at 350 ℃ with MoO_{3-x} as the substrate. The crystal structure of Ru/MoO_{2-x} is explored by XRD (Fig. 2a), and the coexistence of the MoO_2 (PDF#02–0422) and Ru (PDF#65–7645) in Ru/MoO_{2-x} is observed. However, the peaks attributed to MoO_3 can be observed in the XRD pattern of Ru/MoO_3 (Fig. S4), owing to the less content of Ru in Ru/MoO_3. Moreover, in the absence of Ru^{3+}, the MoO_3 phase (PDF#01–0706) rather than MoO_2 phase (PDF#02–0422) is found in MoO_{3-x} after annealing in an Ar/H_2 atmosphere (defined as A-MoO_{3-x}), revealing the transition induced by the introduction of Ru. This transition can be attributed to the interface reaction between Ru and MoO_3 [40,41]. It's worth noting that the MoO_{3-x} can be completely reduced to the MoO_2 phase at 700 ℃ in an Ar/H_2 atmosphere (Fig. S5). The crystal structures are further analyzed using SEM and TEM. As shown in Fig. 2b, Ru/MoO_{2-x} maintains the nanolamellar structure inherited from the precursor MoO_{3-x} substrate, providing a large specific surface area to realize the full exposure of the electroactive sites for facilitating an efficient HER [17,42]. According to the HRTEM patterns (Fig. 2c and S6), the lamellar structures in Ru/MoO_{2-x} presents well-defined lattice fringes with an interlayer spacing of 0.345 nm, which coincides well with the (110) plane of MoO_2. Moreover, Ru nanoclusters can be observed in the red frame of the HRTEM image. This red frame is further analyzed by annular dark-field scanning transmission electron microscopy (ADF-STEM), as presented in Fig. 2d. The ADF-STEM image reveals that the lattice fringes with a pitch of 0.208 nm, indicating the (101) plane of Ru. However, the lattice fringe with a distance of 0.261 nm attributed to the (111) plane of MoO_3 can be still observed in the HRTEM image of Ru/MoO_3 (Fig. S7). These results are consistent with those of the corresponding XRD analysis. In addition, the size distribution of Ru on MoO_2 is observed by HRTEM image as shown in Fig. S8, whose average diameter of the Ru nanoclusters is 1.56 ± 0.63 nm. The selected area electron diffraction pattern (Fig. S9) indicates that the nanocrystals belong to Ru and MoO_2, which is consistent with the above analyses. It is noteworthy that the interface between Ru and MoO_2 is in a high-energy state, because of the high degree of lattice mismatch between Ru and MoO_2, resulting in the formation of abundant defects, which can serve as new catalytic active sites [24,43]. Fig. 2e and S10 reveal that the presence of structural defects in Ru/MoO_{2-x}. In addition, atomic-resolution energy-dispersive X-ray (EDX) line scanning and EDX mapping are detected to analyze the distribution of elements in Ru/MoO_{2-x}. Fig. 2f shows that trace Ru is distributed on the MoO_{2-x} substrate. Moreover, the EDX element mapping images (Fig. 2g) further demonstrate that Ru is uniformly anchored on the MoO_{2-x} substrate. Inductively coupled plasma atomic emission spectrometry (ICP-AES) test reveals the amount of Ru in Ru/MoO_{2-x} as 4.02 wt%, which corresponds well with the EDX results (Fig. S11).

The chemical composition and the surface electronic states of Ru/MoO_{2-x} are analyzed by XPS. As shown in Fig. S12, the XPS survey spectrum confirms the coexistence of Ru, Mo, and O elements in Ru/MoO_{2-x}. To better understand the chemical composition of Ru/MoO_{2-x}, the XPS analysis of A-MoO_{3-x} is performed. The O1s core-level spectra shown in Fig. 3a reveal that more oxygen vacancies exist in Ru/MoO_{2-x}

compared to those in A-MoO_{3-x}. To further confirm the existence of oxygen vacancies in Ru/MoO_{2-x}, the low-temperature electron paramagnetic resonance (EPR) measurement is conducted. As displayed in Fig. S13, a strong signal peak at a g value of 2.003 corroborates the presence of abundant oxygen vacancies [44]. XANES and EXAFS spectroscopies are also performed to study the material structure. As shown in the Fouriertransform (FT) k^2-weighted EXAFS spectra (Fig. 3b), the peak at 1.56 Å corresponds to the Mo-O, and the peak at 2.39 Å conforms to the Mo-Mo. The Mo atom features in Ru/MoO_{2-x} are similar to those in pristine MoO_2. The lower intensity of Mo-O compared to that of MoO_2 is due to the abundant oxygen vacancy defects in Ru/MoO_{2-x} [24,45]. In the Mo K-edge XANES spectra (Fig. 3c), no pre-edge peak at 20006 eV is observed, indicating the absence of MoO_3 in Ru/MoO_{2-x} [46]. In addition, Ru/MoO_{2-x} exhibits negative shifts from MoO_2 to the Mo foil, indicating oxygen vacancy defects in the MoO_2 substrate of Ru/MoO_{2-x}. These results suggest that the introduction of Ru can promote the phase transformation from MoO_3 to MoO_2, as well as the formation of oxygen vacancies in the catalyst. Oxygen vacancies on metal oxides have been demonstrated to increase the electronic conduction of metal oxides and simultaneously enhance the reaction kinetics of metal oxides for the HER [24,25,34,47]. As depicted in the Mo 3d core-level spectra (Fig. S14), Ru/MoO_{2-x} signals exhibit a clear shift to lower binding energies compared to that of A-MoO_{3-x}, implying a low electron density and the existence of the Ru-O-Mo [27,48]. In addition, the binding energy of Ru 3p in the Ru/MoO_{2-x} catalyst is located between that in RuO_2 and the metal Ru (Fig. 3d), indicating that electron transfer occurs from Ru atoms to O atoms in Ru/MoO_{2-x} [34,49]. The EXAFS spectra (Fig. 3e) show that the prepared Ru/MoO_{2-x} possesses two obvious peaks at 1.5 and 2.4 Å, corresponding to Ru-O and Ru-Ru, respectively. Moreover, there is no peak corresponding to Ru-O-Ru at 3.2 Å in the catalyst spectra, thereby confirming the formation of Ru-O-Mo. The positive shifts of the Ru peak of Ru/MoO_{2-x} compared to that of Ru foil (XANES, Fig. 3f), further confirm the substantial electron transfer from Ru atoms to O atoms. The fitting results of Ru K-edge and Mo K-edge EXAFS for Ru/MoO_{2-x} are listed in Table S1. The coordination number (CN) of Ru-Ru in Ru/MoO_{2-x} is lower than that in Ru foil, revealing the coordination environment tends to be unsaturated attributed to the formation of Ru-O-Mo bonds. The low CN of Mo-O is due to the generation of abundant oxygen vacancies in MoO_2 [24]. Moreover, the fitting spectra match well the measured results, further confirming the formation of Ru-O-Mo bonds and oxygen vacancies in MoO_2 (Fig. S15). The Ru-O-Mo sites can significantly improve the H_2O adsorption and dissociation abilities, and enhance the HER performance of the catalyst [34].

3.2. Electrochemical measurement

Owing to the coexistence of Ru nanoclusters, Ru-O-Mo sites, and oxygen-vacancy-enriched MoO_2, the Ru/MoO_{2-x} catalyst can deliver excellent HER performance. Fig. 4a shows the linear sweep voltammetry (LSV) curves, in 1 M KOH, of A-MoO_{3-x}, Ru/MoO_{2-x}, 5 wt% Ru/C, and 20 wt% Pt/C for the HER. The overpotential of Ru/MoO_{2-x} is significantly reduced to 29 mV at a current density of 10 mA cm^{-2} compared to that of A-MoO_{3-x} (549 mV). Moreover, the overpotential of Ru/MoO_{2-x} is also lower than one of Ru/C (45 mV), revealing the enhancement of the HER kinetics by the Ru-O-Mo sites. The polarization curve of MoO_{3-x} is also tested (Figs. S16), indicating its inferior electrochemical performance. Furthermore, the catalytic activity of Ru/MoO_{2-x} is superior to Pt/C. When normalized by the mass of Ru, Ru/MoO_{2-x} presents an excellent mass activity (A g_{Ru}^{-1}), whose current density at a potential of 0.10 V (vs. RHE) is approximately 7.3 times larger than one of the commercial Pt/C (Fig. 4b). The Tafel slope (Fig. 4c and S17) of Ru/MoO_{2-x} is 22 mV dec^{-1}, lower than that of A-MoO_{3-x} (182 mV dec^{-1}), Ru/C (53 mV dec^{-1}), and Pt/C (30 mV dec^{-1}), indicating that the Ru/MoO_{2-x} possesses efficient HER kinetics. The overpotential at 10 mA cm^{-2} and Tafel slope for the obtained catalysts are shown in Fig. 4d. The histograms show the superior catalytic activity of Ru/MoO_{2-x} and its faster reaction kinetics for the HER. To unravel the intrinsic active surface areas of catalysts, the electrochemical surface areas (ECSA) are measured by the cyclic voltammetry (CV) method in non-faradic regions (Fig. S18). ECSA presents a positive correlation relation with the double-layer capacitances (C_{dl}) [10,50]. As shown in Fig. 4e, Ru/MoO_{2-x} delivers a significantly larger C_{dl} value (40.4 mF cm^{-2}) than that of A-MoO_{3-x} (4.6 mF cm^{-2}), indicating that the incorporation of Ru can increase the ECSA of the catalyst to provide sufficient electroactive sites for the HER. The ECSA of Ru/MoO_{2-x} and A-MoO_{3-x} are obtained as 1010 and 115 cm^2, respectively, following the equation ECSA = (C_{dl}*A)/C_s (A is the area of working electrode; C_s =0.04 mF cm^{-2}). The LSV curves normalized by ECSA are shown in Fig. S19, revealing the higher intrinsic activity of Ru/MoO_{2-x} than A-MoO_{3-x}. In addition, the LSV curves show no noticeable changes after 1000 CV cycles for Ru/MoO_{2-x} (Fig. 4 f). To further evaluate the long-term stability of the Ru/MoO_{2-x}, the chronopotentiometry at current density of 1000 mA cm^{-2} are also conducted as shown in Fig. S20. The potential remains almost unchanged after 24 h under 1000 mA cm^{-2}. The phase and morphology of Ru/MoO_{2-x} after the durability test are detected. The SEM images (Fig. S21) and XRD pattern (Fig. S22) of Ru/MoO_{2-x} after the durability test show that its morphology and phase composition remain unchanged even after 1000 cycles of CV. The above results sharply indicate that Ru/MoO_{2-x} has excellent electrochemical stability.

The loading amount of Ru plays an important role in affecting the electrocatalytic HER performance of Ru/MoO_{2-x}. Theoretically, the more loading amount of Ru on MoO_2 substrate, the more superior HER performance can be obtained. However, there is an optimal loading amount of Ru to adequately expose active sites, and the excess Ru will block some inner active sites to deteriorate HER performance. Here, the loading amount of Ru is regulated by adding different concentrations, ranging from 2 to 10 mg mL^{-1}, of $RuCl_3$ solution. As shown in Fig. S21a, the overpotential increases at first and then decreases with an increase in the concentration of the $RuCl_3$ solution. The catalyst with 5 mg mL^{-1} $RuCl_3$ solution exhibits the lowest overpotential at the same current density, the smallest Tafel slope, and the largest ECSA among the three catalysts (Figs. S23–24). The effects of annealing temperature are also analyzed, as presented in Fig. S23. The HER performance of Ru/MoO_{2-x}-T (T represents the annealing temperature ranging from 200 to 700 °C) first increases and then decreases, and the optimal annealing temperature for Ru/MoO_{2-x}-T is 350 °C (Figs. S25–26). Finally, it is comparable with recently reported analogous electrocatalysts in basic electrolytes presented in Fig. 4 g and Table S2, confirming the high catalytic activity of the as-fabricated Ru/MoO_{2-x} toward the HER.

3.3. Mechanism analysis

Finally, the hydrogen evolution process in alkaline electrolyte over Ru/MoO_{2-x} electrocatalyst is speculated. In this work, from the Tafel slope (Fig. 4c), the Ru/MoO_{2-x} conforms to the Volmer-Tafel mechanism in alkaline media. The Tafel slope of 22 mV dec^{-1} reveals that Tafel reaction ($H_{ad} + H_{ad} = H_2$) is the rate-determining step for Ru/MoO_{2-x} in alkaline electrolyte [34,51]. The hydrogen evolution process in alkaline electrolyte over the Ru- and/or MoO_2-based catalysts has been analyzed [34,52–54]. Baek et al. demonstrated that the Ru atoms at the near-interface will promote H_2O adsorption and dissociation [52]. They also proved that the binding energy of Ru-hydrogen on the non-interfacial is lower than that at the near-interface, revealing the non-interfacial Ru sites possess favorable H affinity, while the near-interface Ru sites go against H adsorption. Liu et al. also indicated that Ru-O-Mo sites (Ru atoms at the near-interface) can deliver better H_2O adsorption and dissociation ability than pure Ru [34]. In addition, Ding et al. certified that the oxygen-vacancy-rich MoO_2 can facilitate the decomposition of water to form OH* and H* , and the generated H* will immediately absorb on the Ru nanoparticles closed to the surface [54]. Similarly, the alkaline HER mechanism on Ru/MoO_{2-x} can be

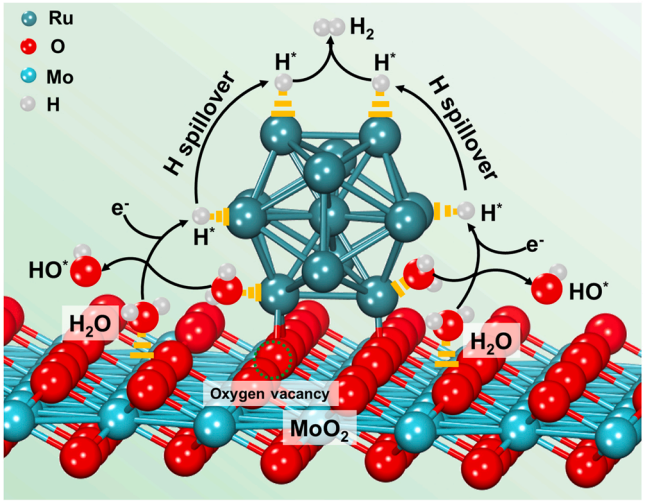

Fig. 5. Mechanism diagram of Ru/MoO_{2-x} for the alkaline HER process.

speculated, as presented in Fig. 5. The Ru-O-Mo sites can promote H-OH bond cleavage to form OH* and H* . Meanwhile, the oxygen-vacancy-enriched MoO_2 can also facilitate the dissociation of water to generate OH* and H* . The non-interfacial Ru sites tend to adsorb H* , and then the H* will migrate from the interfacial Ru sites to the non-interfacial Ru sites via H spillover. Ultimately, the migrated H* on non-interfacial Ru sites will immediately recombine into molecule H_2, which escapes from the catalyst surface [53]. Therefore, it is safe to say that the Ru-incorporated oxygen-vacancy-enriched MoO_2 can lower the energy barrier of H_2O dissociation and promote the desorption step of intermediate H* .

4. Conclusion

In conclusion, we reported an efficient strategy to synthesize the Ru nanoclusters incorporated on oxygen-vacancy-enriched MoO_2 for alkaline HER. The incorporation of Ru into the system can induce a transition from MoO_3 to MoO_2. Moreover, the ADF-STEM, XANES, and EXAFS results indicated the formation of oxygen vacancies and the construction of Ru-O-Mo sites due to the incorporation of Ru nanoclusters. The synergy of Ru nanoclusters and oxygen-vacancy-enriched MoO_2 can lower the energy barrier of H_2O dissociation and facilitate the intermediate desorption, endowing the Ru/MoO_{2-x} catalyst with excellent catalytic activity toward the alkaline HER. Therefore, this study can contribute to designing highly efficient alkaline HER catalysts.

CRediT authorship contribution statement

Chuang Li: Investigation, Methodology, Writing-original draft. **Haeseong Jang**: Methodology, Data curation. **Min Gyu Kim**: Materials characterization. **Liqiang Hou**: Supervision, Writing – review & editing. **Xien Liu**: Project administration, Funding acquisition, Supervision, Writing – review & editing. **Jaephil Cho**: Funding acquisition, Supervision, Writing – review & editing. All authors commented and have given approval to the final version of the manuscript.

Declaration of Competing Interest

The authors declare that they have no known competing financial interests or personal relationships that could have appeared to influence the work reported in this paper.

Acknowledgements

We gratefully acknowledge the financial support from the Taishan Scholar Program of Shandong Province, China (ts201712045) and 2019 Research Fouds of Ulsan National Institute of Science and Technology (1.190002.01).

Appendix A. Supporting information

Supplementary data associated with this article can be found in the online version at doi:10.1016/j.apcatb.2022.121204.

References

[1] X. Zou, Y. Zhang, Noble metal-free hydrogen evolution catalysts for water splitting, Chem. Soc. Rev. 44 (2015) 5148–5180.
[2] J. Suntivich, K.J. May, H.A. Gasteiger, J.B. Goodenough, Y. Shao-Horn, A perovskite oxide optimized for oxygen evolution catalysis from molecular orbital principles, Science 334 (2011) 1383–1385.
[3] W.J. Jiang, T. Tang, Y. Zhang, J.S. Hu, Synergistic modulation of non-precious-metal electrocatalysts for advanced water splitting, Acc. Chem. Res. 53 (2020) 1111–1123.
[4] X. Jiang, H. Jang, S. Liu, Z. Li, M.G. Kim, C. Li, Q. Qin, X. Liu, J. Cho, The heterostructure of Ru_2P/WO_3/NPC synergistically promotes H_2O dissociation for improved hydrogen evolution, Angew. Chem. Int. Ed. 60 (2021) 4110–4116.
[5] B. Zhang, F. Yang, X.D. Liu, N. Wu, S. Che, Y.F. Li, Phosphorus doped nickel-molybdenum aerogel for efficient overall water splitting, Appl. Catal. B-Environ. 298 (2021) 120494–120503.
[6] J. Liang, Q. Liu, T.S. Li, Y.L. Luo, S.Y. Lu, X.F. Shi, F. Zhang, A.M. Asiri, X.P. Sun, Magnetron sputtering enabled sustainable synthesis of nanomaterials for energy electrocatalysis, Green. Chem. 23 (2021) 2834–2867.
[7] L. Zhao, Y. Zhang, Z.L. Zhao, Q.H. Zhang, L.B. Huang, L. Gu, G. Lu, J.S. Hu, L. J. Wan, Steering elementary steps towards efficient alkaline hydrogen evolution via size-dependent Ni/NiO nanoscale heterosurfaces, Natl. Sci. Rev. 7 (2020) 27–36.
[8] Q. Chen, Y. Nie, M. Ming, G.Y. Fan, Y. Zhang, J.S. Hu, Sustainable synthesis of supported metal nanocatalysts for electrochemical hydrogen evolution, Chin. J. Catal. 41 (2020) 1791–1811.
[9] Z. Duan, Y. Sun, W. Zhang, A. Umar, X. Wu, Manipulating electrocatalytic performance of NiCoP nanowire catalyst by V doping in acid-base conditions for hydrogen and oxygen evolution reactions, ACS Appl. Nano Mater. 4 (2021) 10791–10798.
[10] Q. Qin, H. Jang, P. Li, B. Yuan, X. Liu, J. Cho, A tannic acid-derived N-, P-codoped carbon-supported iron-based nanocomposite as an advanced trifunctional electrocatalyst for the overall water splitting cells and zinc-air batteries, Adv. Energy Mater. 9 (2019) 1803312–1803324.
[11] Q. Qin, H. Jang, L. Chen, G. Nam, X. Liu, J. Cho, Low loading of Rh_xP and RuP on N, P codoped carbon as two trifunctional electrocatalysts for the oxygen and hydrogen electrode reactions, Adv. Energy Mater. 8 (2018) 1801478–1801489.
[12] S.Y. Bae, J. Mahmood, I.Y. Jeon, J.B. Baek, Recent advances in ruthenium-based electrocatalysts for the hydrogen evolution reaction, Nanoscale Horiz. 5 (2020) 43–56.
[13] Z. Luo, R. Miao, T.D. Huan, I.M. Mosa, A.S. Poyraz, W. Zhong, J.E. Cloud, D.A. Kriz, S. Thanneeru, J. He, Y. Zhang, R. Ramprasad, S.L. Suib, Mesoporous MoO_{3-x} material as an efficient electrocatalyst for hydrogen evolution reactions, Adv. Energy Mater. 6 (2016) 1600528–1600538.
[14] S. Yuan, Z. Pu, H. Zhou, J. Yu, I.S. Amiinu, J. Zhu, Q. Liang, J. Yang, D. He, Z. Hu, G. Van Tendeloo, S. Mu, A universal synthesis strategy for single atom dispersed cobalt/metal clusters heterostructure boosting hydrogen evolution catalysis at all pH values, Nano Energy 59 (2019) 472–480.
[15] L. Zhang, H. Jang, H. Liu, M.G. Kim, D. Yang, S. Liu, X. Liu, J. Cho, Sodium-decorated amorphous/crystalline RuO_2 with rich oxygen vacancies: a robust pH-universal oxygen evolution electrocatalyst, Angew. Chem. Int. Ed. 60 (2021) 18821–18829.
[16] D. Wu, Y. Wei, X. Ren, X. Ji, Y. Liu, X. Guo, Z. Liu, A.M. Asiri, Q. Wei, X. Sun, Co$(OH)_2$ Nanoparticle-encapsulating conductive nanowires array: room-temperature electrochemical preparation for high-performance water oxidation electrocatalysis, Adv. Mater. 30 (2018) 1705366–1705372.
[17] Y. Jin, H. Wang, J. Li, X. Yue, Y. Han, P.K. Shen, Y. Cui, Porous MoO_2 nanosheets as non-noble bifunctional electrocatalysts for overall water splitting, Adv. Mater. 28 (2016) 3785–3790.
[18] G. Qian, G. Yu, J. Lu, L. Luo, T. Wang, C. Zhang, R. Ku, S. Yin, W. Chen, S. Mu, Ultra-thin N-doped-graphene encapsulated Ni nanoparticles coupled with MoO_2 nanosheets for highly efficient water splitting at large current density, J. Mater. Chem. A 8 (2020) 14545–14554.
[19] J.M. Ge, D.B. Zhang, Y. Qin, T. Dou, M.H. Jiang, F.Z. Zhang, X.D. Lei, Dual-metallic single Ru and Ni atoms decoration of MoS_2 for high-efficiency hydrogen production, Appl. Catal. B-Environ. 298 (2021) 120557–120564.
[20] F. Gong, M. Liu, S. Ye, L. Gong, G. Zeng, L. Xu, X. Zhang, Y. Zhang, L. Zhou, S. Fang, J. Liu, All-pH stable sandwich-structured MoO_2/MoS_2/C hollow nanoreactors for enhanced electrochemical hydrogen evolution, Adv. Funct. Mater. 31 (2021) 2101715–2101724.
[21] W. Hua, H.H. Sun, F. Xu, J.G. Wang, A review and perspective on molybdenum-based electrocatalysts for hydrogen evolution reaction, Rare Met 39 (2020) 335–351.

[22] H. Zeng, S. Chen, Y.Q. Jin, J. Li, J. Song, Z. Le, G. Liang, H. Zhang, F. Xie, J. Chen, Y. Jin, X. Chen, H. Meng, Electron density modulation of metallic MoO_2 by Ni doping to produce excellent hydrogen evolution and oxidation activities in acid, ACS Energy Lett. 5 (2020) 1908–1915.
[23] X. Li, J. Yu, J. Jia, A. Wang, L. Zhao, T. Xiong, H. Liu, W. Zhou, Confined distribution of platinum clusters on MoO_2 hexagonal nanosheets with oxygen vacancies as a high-efficiency electrocatalyst for hydrogen evolution reaction, Nano Energy 62 (2019) 127–135.
[24] J. Cai, J. Ding, D. Wei, X. Xie, B. Li, S. Lu, J. Zhang, Y. Liu, Q. Cai, S. Zang, Coupling of Ru and O-vacancy on 2D Mo-based electrocatalyst via a solid-phase interface reaction strategy for hydrogen evolution reaction, Adv. Energy Mater. 11 (2021) 2100141–2100149.
[25] Y. Qiu, S. Liu, C. Wei, J. Fan, H. Yao, L. Dai, G. Wang, H. Li, B. Su, X. Guo, Synergistic effect between platinum single atoms and oxygen vacancy in MoO_2 boosting pH-universal hydrogen evolution reaction at large current density, Chem. Eng. J. 427 (2022) 131309–131318.
[26] B. Wang, Z. Zhang, S. Zhang, Y. Cao, Y. Su, S. Liu, W. Tang, J. Yu, Y. Ou, S. Xie, J. Li, M. Ma, Surface excited MoO_2 to master full water splitting, Electrochim. Acta 359 (2020) 136929–136935.
[27] N. Yuan, Q. Jiang, Z. Wu, J. Tang, Ru nanoparticles decorated on 2D MoO_2 nanosheets as efficient and durable electrocatalysts for the hydrogen evolution reaction in a wide pH range, J. Phys. Chem. C. 124 (2020) 10804–10814.
[28] P. Jiang, Y. Yang, R. Shi, G. Xia, J. Chen, J. Su, Q. Chen, Pt-like electrocatalytic behavior of Ru-MoO_2 nanocomposites for the hydrogen evolution reaction, J. Mater. Chem. A 5 (2017) 5475–5485.
[29] L. Yang, J. Yu, Z. Wei, G. Li, L. Cao, W. Zhou, S. Chen, Co-N-doped MoO_2 nanowires as efficient electrocatalysts for the oxygen reduction reaction and hydrogen evolution reaction, Nano Energy 41 (2017) 772–779.
[30] T. Qiu, Z. Liang, W. Guo, S. Gao, C. Qu, H. Tabassum, H. Zhang, B. Zhu, R. Zou, Y. Shao-Horn, Highly exposed ruthenium-based electrocatalysts from bimetallic metal-organic frameworks for overall water splitting, Nano Energy 58 (2019) 1–10.
[31] J. Ding, Q. Shao, Y. Feng, X. Huang, Ruthenium-nickel sandwiched nanoplates for efficient water splitting electrocatalysis, Nano Energy 47 (2018) 1–7.
[32] C. Clay, S. Haq, A. Hodgson, Intact and dissociative adsorption of water on Ru (0001), Chem. Phys. Lett. 388 (2004) 89–93.
[33] S. Maier, I. Stass, J.I. Cerda, M. Salmeron, Unveiling the mechanism of water partial dissociation on Ru(0001), Phys. Rev. Lett. 112 (2014) 126101–126105.
[34] H. Li, K. Liu, J. Fu, K. Chen, K. Yang, Y. Lin, B. Yang, Q. Wang, H. Pan, Z. Cai, H. Li, M. Cao, J. Hu, Y.R. Lu, T.S. Chan, E. Cortés, A. Fratalocchi, M. Liu, Paired Ru-O-Mo ensemble for efficient and stable alkaline hydrogen evolution reaction, Nano Energy 82 (2021) 105767–105774.
[35] Z. Liu, L. Zeng, J. Yu, L. Yang, J. Zhang, X. Zhang, F. Han, L. Zhao, X. Li, H. Liu, W. Zhou, Charge redistribution of Ru nanoclusters on Co_3O_4 porous nanowire via the oxygen regulation for enhanced hydrogen evolution reaction, Nano Energy 85 (2021) 105940–105948.
[36] S. Zhang, H. Yang, H. Huang, H. Gao, X. Wang, R. Cao, J. Li, X. Xu, X. Wang, Unexpected ultrafast and high adsorption capacity of oxygen vacancy-rich WO_x/C nanowire networks for aqueous Pb^{2+} and methylene blue removal, J. Mater. Chem. A 5 (2017) 15913–15922.
[37] J. Xu, C. Zhang, H. Liu, J. Sun, R. Xie, Y. Qiu, F. Lü, Y. Liu, L. Zhuo, X. Liu, J. Luo, Amorphous MoO_x-stabilized single platinum atoms with ultrahigh mass activity for acidic hydrogen evolution, Nano Energy 70 (2020) 104529–104536.
[38] H. Cheng, T. Kamegawa, K. Mori, H. Yamashita, Surfactant-free nonaqueous synthesis of plasmonic molybdenum oxide nanosheets with enhanced catalytic activity for hydrogen generation from ammonia borane under visible light, Angew. Chem. Int. Ed. 53 (2014) 2910–2914.
[39] S. Zhang, G. Wang, J. Jin, L. Zhang, Z. Wen, J. Yang, Self-catalyzed decomposition of discharge products on the oxygen vacancy sites of MoO_3 nanosheets for low-overpotential Li-O_2 batteries, Nano Energy 36 (2017) 186–196.
[40] L. Qiu, K. Chen, D. Yang, M. Zhang, X. Hao, W. Li, J. Zhang, W. Wang, Metal copper induced the phase transition of MoO_3 to MoO_2 thin films for the CdTe solar cells, Mat. Sci. Semicon. Proc. 122 (2021) 105475–105485.
[41] J. Zhang, X. Xu, L. Yang, D. Cheng, D. Cao, Single-atom Ru doping induced phase transition of MoS_2 and S vacancy for hydrogen evolution reaction, Small Methods 3 (2019) 1900653–1900661.
[42] S. Geng, Y. Liu, Y.S. Yu, W. Yang, H. Li, Engineering defects and adjusting electronic structure on S doped MoO_2 nanosheets toward highly active hydrogen evolution reaction, Nano Res. 13 (2019) 121–126.
[43] X. Chen, G. Liu, W. Zheng, W. Feng, W. Cao, W. Hu, P. Hu, Vertical 2D MoO_2/$MoSe_2$ core-shell nanosheet arrays as high-performance electrocatalysts for hydrogen evolution reaction, Adv. Funct. Mater. 26 (2016) 8537–8544.
[44] L. Hou, W. Yang, X. Xu, B. Deng, J. Tia, S. Wang, F. Yang, Y. Li, *In-situ* formation of oxygen-vacancy-rich $NiCo_2O_4$/nitrogen-deficient graphitic carbon nitride hybrids for high-performance supercapacitors, Electrochim. Acta 340 (2020) 135996–136005.
[45] K. Tu, D. Tranca, F. Rodriguez-Hernandez, K. Jiang, S. Huang, Q. Zheng, M. X. Chen, C. Lu, Y. Su, Z. Chen, H. Mao, C. Yang, J. Jiang, H.W. Liang, X. Zhuang, A novel heterostructure based on RuMo nanoalloys and N-doped carbon as an efficient electrocatalyst for the hydrogen evolution reaction, Adv. Mater. 32 (2020) 2005433–2005442.
[46] S. Macis, J. Rezvani, I. Davoli, G. Cibin, B. Spataro, J. Scifo, L. Faillace, A. Marcelli, Structural evolution of MoO_3 thin films deposited on copper substrates upon annealing: an X-ray absorption spectroscopy study, Condens. Matter. 4 (2019) 41–47.
[47] T. Zhang, M.Y. Wu, D.Y. Yan, J. Mao, H. Liu, W.B. Hu, X.W. Du, T. Ling, S.Z. Qiao, Engineering oxygen vacancy on NiO nanorod arrays for alkaline hydrogen evolution, Nano Energy 43 (2018) 103–109.
[48] C. Wang, L. Qi, Heterostructured inter-doped ruthenium-cobalt oxide hollow nanosheet arrays for highly efficient overall water splitting, Angew. Chem. Int. Ed. 59 (2020) 17219–17224.
[49] L. Deng, F. Hu, M. Ma, S.C. Huang, Y. Xiong, H.Y. Chen, L. Li, S. Peng, Electronic modulation caused by interfacial Ni-O-M (M=Ru, Ir, Pd) bonding for accelerating hydrogen evolution kinetics, Angew. Chem. Int. Ed. 133 (2021) 22450–22456.
[50] Q. Qin, H. Jang, Y. Wang, L. Zhang, Z. Li, M.G. Kim, S. Liu, X. Liu, J. Cho, Gettering La effect from La_3IrO_7 as a highly efficient electrocatalyst for oxygen evolution reaction in acid media, Adv. Energy Mater. 11 (2020) 2003561–2003567.
[51] J. Peng, Y. Chen, K. Wang, Z. Tang, S. Chen, High-performance Ru-based electrocatalyst composed of Ru nanoparticles and Ru single atoms for hydrogen evolution reaction in alkaline solution, Int. J. Hydrog. Energy 45 (2020) 18840–18849.
[52] J. Mahmood, F. Li, S.M. Jung, M.S. Okyay, I. Ahmad, S.J. Kim, N. Park, H.Y. Jeong, J.B. Baek, An efficient and pH-universal ruthenium-based catalyst for the hydrogen evolution reaction, Nat. Nanotechnol. 12 (2017) 441–446.
[53] M.M. Lao, G.Q. Zhao, P. Li, T.Y. Ma, Y.Z. Jiang, H.G. Pan, S.X. Dou, W.P. Sun, Manipulating the coordination chemistry of Ru-N(O)-C moieties for fast alkaline hydrogen evolution kinetics, Adv. Funct. Mater. 31 (2021) 2100698–2100706.
[54] J.L. Cai, J. Ding, D.H. Wei, X. Xie, B.J. Li, S.Y. Lu, J.M. Zhang, Y.S. Liu, Q. Cai, S. Q. Zang, Coupling of Ru and O-vacancy on 2D Mo-based electrocatalyst via a solid-phase interface reaction strategy for hydrogen evolution reaction, Adv. Energy Mater. 11 (2021) 2100141–2100149.